Drift ratchet

Christiane Kettner,[1] Peter Reimann,[1] Peter Hänggi,[1] and Frank Müller[2]
[1]*Universität Augsburg, Institut für Physik, Universitätsstrasse 1, D-86135 Augsburg, Germany*
[2]*Max-Plank-Institut für Mikrostrukturphysik, Weinberg 2, 06120 Halle, Germany*
(Received 23 July 1999)

We consider a silicon wafer, pierced by millions of identical pores with periodically varying diameters but without spatial inversion symmetry (ratchet profile). When a liquid is periodically pumped back and forth through the pores, our theory predicts a net transport of suspended micrometer-sized particles (drift ratchet). The direction of this particle current depends very sensitively on the size of the particles. For typical parameter values of the experiment, two different types of particles at an initially homogeneous 1:1 mixture are spatially separated with a purity beyond 1:1000 on a time scale of a few hours in comparably large quantities. This result is due to the highly parallel architecture of the device. The experimental realization of the setup, presently under construction, thus appears to be a promising new particle separation device, possibly superior to existing methods for particles sizes on the micrometer scale.

PACS number(s): 05.40.−a, 07.10.Cm, 87.80.−y

I. INTRODUCTION

Is it possible, and how is it possible, to convert unbiased random fluctuations into directed motion if all acting forces and temperature gradients average out to zero? A systematic exploration of this provocative question [1] was initiated almost simultaneously by three independent groups [2] and has been attracting a lot of excitement under the label of ''molecular motor,'' ''Brownian motor,'' or ''ratchet'' ever since [3]. Besides the intriguing fundamental aspects of such far from equilibrium systems, e.g., with respect to the second law of thermodynamics and Maxwell's demon, their potential relevance with respect to intracellular transport mechanisms [4], transport in noncentrosymmetric materials [5], and technological applications as particle pumps and separation devices [6] have been major driving forces of those investigations right from the beginning [2,3]. It is the latter objective which is the focus of our present paper in that the theoretical framework of a novel ratchet-type particle separation device, presently under construction in the laboratories of the Max-Planck-Institut in Halle (Germany), is outlined.

The practical realizability of particle transport in manmade devices has been demonstrated experimentally for several variants of the ratchet concept [7]. The experimental setup we have in mind goes one step further in that millions of identical ratchets are operating simultaneously in parallel with the perspective of pumping and separating for the first time relatively large quantities of micrometer-sized particles on a reasonable time scale. In particular, in comparison to the widespread electrophoretic separation techniques [8], our present device works appreciably faster and can be reused. The particles are furthermore dispersed in a liquid, e.g., water, in contrast to the inconvenient gel and polymer solutions required in electrophoresis. Compared with methods based on the field-flow fractionation scheme [9], which appears to have a rather limited separating power for particles in the range of 0.5–1 μm, our present theory predicts a fairly high resolution in this range of particle sizes, indicating that the real device may indeed become a separation method of broad practical interest.

The outline of our paper is as follows: In Sec. II, the experimental setup is described and in Sec. III a theoretical model for the particle dynamics in a single infinitely long ratchet-shaped pore is introduced. In Sec. IV, numerical solutions of this model dynamics—the so-called drift ratchet—are presented and discussed. The complication that the real pores are of finite length and connected at both ends with finite reservoirs is taken into account in Sec. V. For this case, a coarse-grained description of the drift ratchet dynamics is put forward and solved by numerical and analytical means. A summary and outlook is presented in Sec. VI.

II. SETUP

The experimental situation which we wish to theoretically describe in this paper is depicted in Figs. 1–3. The main component of the setup is a piece of silicon—a so-called silicon wafer—pierced by a huge number of practically identical and parallel pores, each of a few micrometers in diameter (Fig. 1). (For convenience, we will take the pore axis as the z axis of our coordinate frame.) The art of fabricating such a macroporous silicon wafer is described in detail in [10]. Especially, by means of very sophisticated techniques it is possible to periodically vary the diameter of the pores along their axis in a controlled manner [10]. Having in mind a ratchetlike pumping device for microparticles, the periodic variations of the pore profile are furthermore chosen asymmetric under spatial inversion (Fig. 2). In order to practically eliminate gravitational effects and the tendency of the particles to stick to the pore walls and to each other, the particles are suspended in a liquid (e.g., water). [Moreover, due to its compressibility, the dynamics of a gas instead of a liquid inside the pores would be theoretically much more difficult to solve; see Sec. III C.] Finally, the silicon wafer is connected at both ends to basins of the liquid-plus-particle suspension (Fig. 3).

To establish contact with previously studied ratchet models [2,3], the first idea that comes to mind is to bring into play some time-dependent electrical fields. However, since silicon already has a noticeable conductivity at room tem-

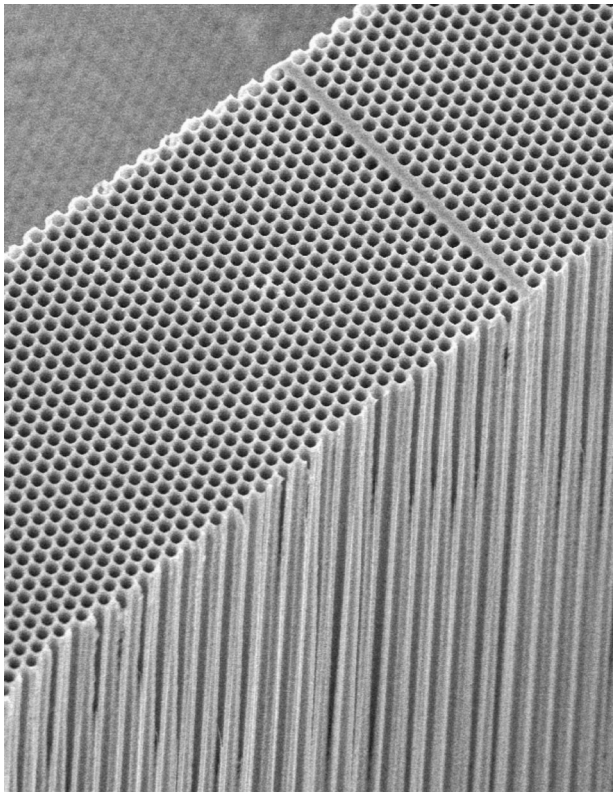

FIG. 1. Scanning-electron-microscope picture of silicon, pierced by a huge number of practically identical pores with pore distances of 1.5 μm and pore diameters of 1 μm.

perature, all electrical fields will be almost completely shielded inside the silicon wafer. Moreover, the electrical charge of the microparticles is strongly dependent on the fluid in which they are suspended and may vary too much to allow for a satisfactory separation. For these reasons, we have abandoned the use of electrical fields and instead created the far-from-equilibrium situation—necessary for the functioning of any ratchet mechanism [3]—by periodically pumping the liquid back and forth through the pores. Ratchet models in the presence of a time-periodic external force have been studied in [11], while a ratcheting mechanism based on the hydrodynamic effect of the so-called Stokes drift (particles are ''surfing'' on traveling waves) has been addressed in [12]. Though these models share some aspects with our present system, they are of no direct use for the following reasons: (i) Unlike in almost all previous models [2,3], no ''ratchet *potential* '' is involved in our case. (ii) The dynamics within a single pore is still a complicated three-dimensional problem that cannot be reduced *a priori* to an effective one-dimensional description.

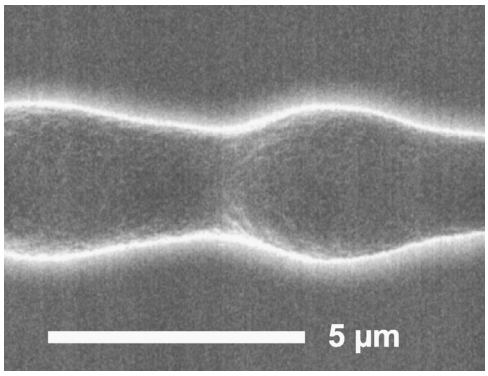

FIG. 2. Scanning-electron-microscope picture of a single pore with a ratchet-shaped (periodic but asymmetric) variation of the diameter along the pore axis (z axis).

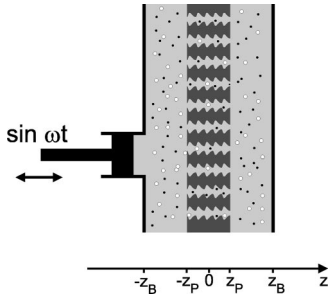

FIG. 3. Schematic cross section through the x-z plane of the experimental setup. The macroporous silicon wafer, extending from $-z_P$ to z_P, is connected at both ends to basins. The pores with their ratchet-shaped profile along the z axis (see Fig. 2) are schematically indicated in dark grey. The basins and the pores are filled with liquid and micrometer-sized particles (two different species are indicated), pumped back and forth by a pumping device (indicated by the piston on the left hand side; omitted is a similar piston or a membrane at the right basin boundary, required to keep the liquid-volume constant). In the real experiment, the length $2z_P$ of the wafer along the z axis (and thus of the single pores) is 100–200 μm and the length $z_B - z_P$ of each basin is 20–200 μm. The extension of the device along the x axis is about 1–2 cm and similarly along the y direction. The corresponding number of pores is about 1.5×10^6–6×10^6.

III. INFINITE PORE MODEL

In this section we introduce a theoretical description of the particle motion in a single infinitely long pore under the idealizing assumptions that the suspension is sufficiently diluted such that particle interaction effects are negligible and that the interaction with the pore walls can be captured by perfectly reflecting boundary conditions. We furthermore assume strict periodicity of the pore profile, a perfectly rigid, spherical shape of the particles, and incompressibility of the liquid. In order to solve this idealized model, we shall proceed in two steps: In Sec. III A we assume that a certain time-dependent velocity field $\vec{v}(\vec{x},t)$ inside the pores is given, on the basis of which we then establish the stochastic model dynamics of a suspended particle under the action of the thermal noise. In an intermitting Sec. III B we give an intuitive argument of why a ''ratchet effect,'' i.e., the emergence of a net particle current in some preferential direction, may be expected for such a stochastic dynamics. Section III C complements the model by addressing the problem of how to determine the deterministic velocity field $\vec{v}(\vec{x},t)$ for a sinusoidal pumping of the liquid-plus-particle suspension through the pore. The quantitative numerical solution of this quite involved combination of hydrodynamic and stochastic problems is postponed to Sec. IV.

A. Stochastic dynamics

We consider a single spherical particle in a fluid that is periodically pumped back and forth through an infinitely

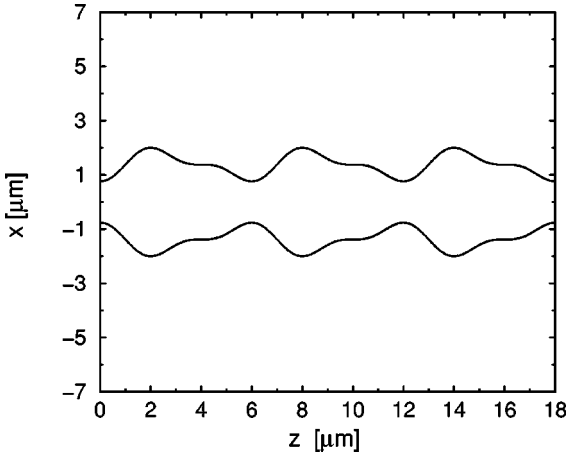

FIG. 4. Cross-section (x-z plane) through a single pore with z-dependent radius according to Eq. (2).

long pore. For the typical parameter values of the real experiment one readily finds that buoyancy effects due to the influence of gravitation as well as inertia effects of the particle are negligibly small; i.e., the particle dynamics in the viscous liquid is strongly overdamped. Assuming that the three-dimensional time-dependent velocity field $\vec{v}(\vec{x},t)$ of the liquid is given, the particle with coordinate $\vec{x}(t) = (x(t),y(t),z(t))$ is governed by the deterministic dynamics $\dot{\vec{x}}(t)=\vec{v}(\vec{x}(t),t)$. To be precise, $\vec{v}(\vec{x},t)$ is here in fact not the velocity field of the fluid alone but rather the speed with which a spherical particle with center at $\vec{x}(t)$ and a small but finite radius is carried along by the surrounding liquid (see Sec. III C). This dynamics induced by the streaming liquid has to be complemented by proper boundary conditions at the pore walls, which we model as perfectly reflecting boundary conditions, and by the diffusion of the micrometer-sized particle due to random thermal fluctuations $\vec{\xi}(t)$. These random forces, stemming from the impacts of the surrounding liquid molecules, can be described in the common way by Gaussian white noise. We thus end up with the following Langevin model equation for the trajectory $\vec{x}(t)$ of a microsphere inside a single pore:

$$\dot{\vec{x}}(t)=\vec{v}(\vec{x}(t),t)+\sqrt{2D_{th}}\vec{\xi}(t). \tag{1}$$

Here, $D_{th}:=kT/\eta$ is the thermal diffusion coefficient, with the temperature T (kept constant at room temperature), the Boltzmann constant k, and Stokes' friction coefficient η. The latter is given by $6\pi R\nu$ in leading order in the Reynolds number R_e, with the sphere's radius R and the viscosity of the liquid ν. The vector components $\xi_i(t)$, $i=1,2,3$, of the noise $\vec{\xi}(t)$ are independent Gaussian stochastic processes with $\langle\xi_i(t)\rangle=0$ and $\langle\xi_i(t)\xi_j(t')\rangle=\delta(t-t')\delta_{ij}$.

The time and space dependence of the velocity field $\vec{v}(\vec{x}(t),t)$ arises from the periodical pumping of the carrier liquid through a pore with periodically but asymmetrically changing diameter. As a concrete working model for the ratchet-shaped profile of the pores we assume a variation of the pore radius $r_p(z)$ along the pore axis (z axis) of the form (see Fig. 4)

$$r_p(z)=\frac{1}{2.1}\left[2.9+\sin[\phi(z)]+\frac{1}{2}\sin[2\phi(z)]\right]\ \mu\text{m},$$

$$\phi(z):=2\pi z/L-\pi/3,\quad L=6\ \mu\text{m}. \tag{2}$$

The reflecting boundary condition in particular encompasses the requirement that the entire spherical particle with center $\vec{x}(t)$ and some finite radius never exceed the pore boundaries from Eqs. (2).

B. Ratchet effect

Clearly, after one period of driving, the liquid in the pore returns (after averaging over thermal fluctuations) to the same position from where it started out. Why should we not expect the same null effect for the suspended particles? Under various comparable conditions, the emergence of such a systematic particle transport has indeed been documented in detail, e.g., in [2,3,7,11,12] and further references therein, with the main conclusion that under far-from-equilibrium conditions, periodicity in combination with spatial asymmetry is generically sufficient for the manifestation of this so-called ''ratchet effect.'' These preconditions are all given in our setup as well; especially the far-from-equilibrium situation is created by the periodical pumping of the liquid through the pore. The crucial difference between a particle and the liquid is its finite extension. First, the speed of the particle in general does not exactly agree with that of the liquid at the center of the particle if this particle were not present. Due to spatial asymmetry, there is no reason why the net displacement of the particle by diffusing randomly between liquid layers of different speeds (similarly as in the so-called Taylor dispersion [13]) should after one driving period average out exactly to zero like for the liquid. Second, the finite radius implies collisions with the pore walls, which again alter the dynamical behavior of the particles in comparison with that of the liquid.

While for finite particle sizes we thus expect generically a finite net particle current, in the limit of a vanishing radius the particles behave like the liquid and the current disappears. On the other hand, too large particles will no longer be able to pass through the bottlenecks of the ratchet-shaped pores, giving rise again to a zero current.

C. Computation of the velocity field

The first step towards a quantitative solution of the stochastic dynamics (1) consists in calculating the velocity field $\vec{v}(\vec{x},t)$ caused by the liquid flow through the pores. For this purpose, we start with the Navier–Stokes equation in the following dimensionless form [14]:

$$R_e\left[\frac{1}{S}\frac{\partial\vec{v}'}{\partial t'}+(\vec{v}'\cdot\vec{\nabla}')\cdot\vec{v}'\right]=-\vec{\nabla}'p'+\Delta'\vec{v}', \tag{3}$$

supplemented by the continuity equation for the incompressible liquid $\vec{\nabla}\cdot\vec{v}'=0$ and the boundary conditions $\vec{v}'=\vec{0}$ at the pore walls. Here, the primed dimensionless quantities are related to the original dimensionful ones by $\vec{v}'=\vec{v}/v_c$, $t'=t\omega/2\pi$, $\vec{x}'=\vec{x}/r_{min}$, $\nabla'=r_{min}\nabla$, and $p'=pr_{min}/(\nu v_c)$.

Furthermore, the arguments $\vec{x}'$ and t' of the functions $\vec{v}'$ and p' have been omitted. The velocity scale v_c is given by the maximal velocity of the liquid (typically 2–9 mm/s for $\omega/2\pi = 40-100$ Hz, $A = L-3L$, see below), r_{min} is the minimal pore radius [0.76 μm for the example (2)], and $\omega/2\pi$ is the pumping frequency (typically 40–100 Hz).

The coefficients R_e and S in Eq. (3) denote the dimensionless so-called Reynolds and Strouhal numbers, respectively, defined as $R_e := v_c \rho_l r_{min}/\nu$ and $S := 2\pi v_c/\omega r_{min}$, with the liquid density ρ_l. Under typical experimental conditions the Reynolds number R_e is found to be in the range of 10^{-3}–10^{-2} and the Strouhal number S is about 10^2. Due to $R_e \ll 1$ and $R_e/S \ll 1$, the left hand side in Eq. (3) can be neglected, which leaves us with the so-called ''creeping flow equations'' [14]

$$\Delta \vec{v}(\vec{x},t) = \vec{\nabla} p(\vec{x},t). \tag{4}$$

Here and in the following paragraphs we have dropped the primes but continue to work in dimensionless units. The physical picture behind the above approximation is that the friction terms are dominant over the inertia terms and that the flow is able to adapt instantaneously to the time variations of the pressure field $p(\vec{x},t)$. In the presence of a sinusoidal pumping with frequency $\omega/2\pi$, this pressure field takes the form

$$p(\vec{x},t) = p_0(\vec{x}) \sin(2\pi t). \tag{5}$$

Note that within the creeping flow approximation (4), the resulting time dependence of the velocity field is merely parametric. In other words, once a solution $\vec{v}_0(\vec{x})$ has been determined for the steady pressure field $p_0(\vec{x})$, i.e.,

$$\Delta \vec{v}_0(\vec{x}) = \vec{\nabla} p_0(\vec{x}), \tag{6}$$

the solution $\vec{v}(\vec{x},t)$ at any time t is simply given by

$$\vec{v}(\vec{x},t) = \vec{v}_0(\vec{x}) \sin(2\pi t). \tag{7}$$

A convenient strategy to solve the time-independent creeping flow equations (6) is by means of the so-called vector potential $\vec{\mathcal{A}}(\vec{x})$, implicitly defined via $\vec{v}_0(\vec{x}) = \vec{\nabla} \times \vec{\mathcal{A}}(\vec{x})$. The continuity equation for the incompressible liquid $\vec{\nabla} \cdot \vec{v}_0(\vec{x}) = 0$ on the one hand guarantees the existence of such a vector potential $\vec{\mathcal{A}}(\vec{x})$ and on the other hand is automatically fulfilled in this way. Eliminating $\vec{v}(\vec{x})$ in favor of $\vec{\mathcal{A}}(\vec{x})$ in Eq. (6) and then taking the rotation on both sides leads us to the linear homogeneous equation

$$\Delta^2 \vec{\mathcal{A}}(\vec{x}) = \vec{0}. \tag{8}$$

Next we go over the cylinder coordinates $(x,y,z) \mapsto (r,z,\phi)$ and corresponding velocity components (v_r, v_z, v_ϕ), defined through

$$\vec{v}_0 = v_r \vec{e}_r + v_z \vec{e}_z + v_\phi \vec{e}_\phi. \tag{9}$$

Note that $v_r = [v_x^2 + v_y^2]^{1/2}$ and that we have dropped the index ''0'' in (v_r, v_z, v_ϕ). We assume that the solution $\vec{v}_0(r,z,\phi)$ respects both the cylinder symmetry and the discrete translational symmetry of the system, i.e., $\vec{v}_0(r,z,\phi) = \vec{v}_0(r,z)$, independent of ϕ, $v_\phi(r,z) \equiv 0$, $\vec{v}_0(r,z+L) = \vec{v}_0(r,z)$, and $\partial v_z(r=0,z)/\partial r = 0$. The assumption that the solution does not spontaneously break the symmetry of the system is quite plausible and is further corroborated by the fact that we will indeed find such a solution in the following; if the solution were unique, this in fact would rigorously justify the above assumptions. The linearity of Eqs. (6) and (8) reflects the fact that we are in the deep laminar (nonturbulent) regime and thus indeed suggests a unique solution of the liquid flow for a given pressure drop per spatial period L.

Note that, much like in classical electrodynamics, $\vec{v}_0(\vec{x})$ fixes the vector potential $\vec{\mathcal{A}}(\vec{x})$ only up to a gauge freedom. Exploiting this freedom and the ϕ independence of the vector potential one can prove [14] the existence of a scalar field $\Psi(r,z)$ with the properties that $\vec{\mathcal{A}}(r,z) = \Psi(r,z)\,\vec{e}_\phi/r$ and that lines of constant Ψ are everywhere tangent to the velocity field (hence Ψ is also named the ''streamline function''). In terms of Ψ, the velocity field is now given by

$$\vec{v}_0(r,z) = \vec{\nabla} \times [\Psi(r,z)\vec{e}_\phi/r]. \tag{10}$$

Substituting $\vec{\mathcal{A}}(r,z) = \Psi(r,z)\,\vec{e}_\phi/r$ in Eq. (8) one arrives at the following linear homogeneous fourth order equation for the streamline function:

$$\hat{L}\Psi(r,z) = 0, \quad \hat{L} := \left[r \frac{\partial}{\partial r} \frac{1}{r} \frac{\partial}{\partial r} + \frac{\partial^2}{\partial z^2} \right]^2. \tag{11}$$

From the boundary and symmetry conditions for $\vec{v}(r,z)$ the following boundary conditions for the streamline function can be derived:

$$\Psi(r=0,z) = c, \tag{12}$$

$$\frac{\partial^{2n+1}}{\partial r^{2n+1}} \Psi(r=0,z) = 0, \quad n = 0,1, \tag{13}$$

$$\vec{\nabla} \Psi(r = r_p(z), z) = \vec{0}, \tag{14}$$

$$\Psi(r,z+L) = \Psi(r,z). \tag{15}$$

Once a solution of Eqs. (11)–(15) with an arbitrary constant c in Eq. (12) has been found, the velocity field $\vec{v}_0(\vec{x})$ is determined by Eq. (10) up to a multiplicative factor. Due to the linearity of Eqs. (6), (10), and (11), this factor together with the pressure field $p_0(\vec{x})$ can finally be obtained as follows: We define the pressure drop δp_0 over one spatial period by

$$\delta p_0 := p_0(r,z) - p_0(r,z+L). \tag{16}$$

Note that the sign convention in Eq. (16) is chosen such that a positive δp_0 will cause a liquid flow to the right (in the positive z direction). Further, δp_0 is indeed independent of r and z due to Eq. (6) and $\vec{v}_0(r,z+L) = \vec{v}_0(r,z)$ and can be rewritten as

$$\delta p_0 = -2\int_0^L \frac{\partial^2}{\partial r^2} v_z(r=0,z)\,dz. \tag{17}$$

Given δp_0, the multiplicative factor of the velocity field is now fixed by Eq. (17).

We remark that in the infinite pore limit the pressure drop δp_0 over one period is the only free parameter in the problem (6). In contrast, for a finite pore, the pressure field needs in general no longer agree with the infinite pore solution $p_0(r,z)$ near the ends of the pore [15], but will quickly converge towards $p_0(r,z)$ as the distance from the pore ends increases.

Instead of the pressure drop δp_0 we will later use the equivalent parameter, $A=\int_0^{T_p/2} V_z[r=0,z(t),t]dt$, with T_p being the period of driving, defined as the amplitude (maximal elongation) of the liquid around the reference position $r=z=0$.

By closer inspection of Eqs. (11)–(15) the following analytical approximation, valid for small variations of $r_p(z)$, can be derived:

$$\Psi(r,z) = c - \frac{1}{2}\left(\frac{r}{r_p(z)}\right)^2 + \frac{1}{4}\left(\frac{r}{r_p(z)}\right)^4. \tag{18}$$

This approximation, which becomes exact for a constant $r_p(z)$, can be used to roughly estimate the pressure drop δp_0 for a given amplitude A. However, for the purpose of numerical simulations in Eq. (1) with Eq. (2) the accuracy of the approximation (18) is not sufficient, and a numerical solution of Eqs. (11)–(15) becomes necessary. To this end, we have adopted a modified relaxation scheme according to the following recursion relation:

$$\Psi^{(n+1)}(r,z) = \Psi^{(n)}(r,z) - \alpha\cdot\hat{L}\Psi^{(n)}(r,z). \tag{19}$$

Note that on a discretized r-z lattice, the corresponding discretized operator (11) is no longer uniquely fixed at the borders $r=0$ and $r=r_p(z)$ of the lattice. This ambiguity is removed by taking into account the boundary conditions (12)–(14). The boundary condition (15) is automatically fulfilled if it is satisfied by the initial function $\Psi^{(0)}(r,z)$. The constant α in Eq. (19) must be chosen positive but sufficiently small; otherwise the iteration scheme diverges. On our standard r-z lattice of 250×750 sites, a value of $\alpha\leqslant 0.09$ has proved to work well. Since the convergence is not very fast, it is advantageous to start with a coarse grid and then steadily proceed to finer and finer grids.

Figures 5 and 6 give an impression of the solution $\vec{v}_0(r,z)$ in cylinder coordinates [cf. Eq. (9)] and dimensionful units, which has been obtained numerically in the way described above: While $v_\phi(r,z)$ is identically zero, the velocity components $v_r(r,z)$ and $v_z(r,z)$ exhibit the typical ratchet form when drawn as a function of z (Fig. 5.) Note, however, that in contrast to most previously studied ratchet systems [2,3], these functions characterize here a velocity field, not a ''ratchet *potential*.'' As a function of r, the component $v_z(r,z)$ takes its maximum in the center of the pore (Fig. 6), while the radial velocity $v_r(r,z)$ is maximal at about half the local pore radius.

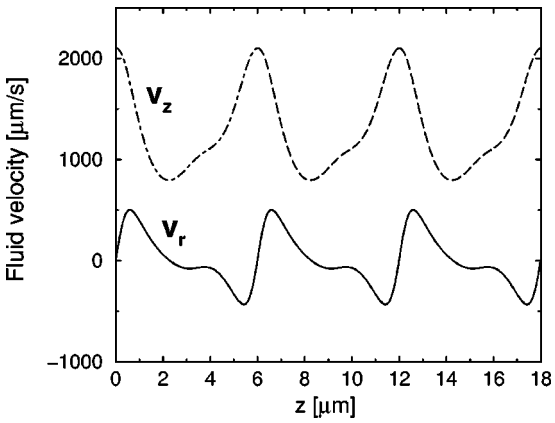

FIG. 5. The components $v_r(r,z)$ and $v_z(r,z)$ of the liquid velocity field (9) inside an infinitely long pore (2) (see also Fig. 4) as a function of z at a fixed r value of $3\,r_{min}/4$. The viscosity ν is $0.5\,\nu_{water}$ and the pressure drop δp_0 per period L from Eqs. (16) and (17) is about 7.6 Pa. The corresponding pumping amplitude A (see main text for the exact definition) is $A=2L=12$ μm and $\omega/2\pi=40$ Hz.

Thus far we have restricted ourselves to the velocity field of the liquid through a pore in the absence of any therein suspended particles. However, what actually counts in the overdamped stochastic dynamics (1) is the velocity with which a particle is carried along by the surrounding liquid. For a finite particle radius, this velocity field can strictly speaking only be obtained by solving the hydrodynamics of the compound liquid-plus-particle system. Practically, this problem is beyond what can be done numerically or analytically. Moreover, by including thermal fluctuation effects as in Eq. (1), a truly rigorous approach is possible only on the basis of a kinetic description like the Boltzmann equation, which even more so is way beyond practicability. Hence we keep staying with our phenomenological combined stochastic-hydrodynamical description, well established [12,13] since Einstein's Brownian motion theory, with the following approximations for the relevant velocity field in Eq. (1): First, we neglect back reactions of the particle on the flow of the liquid. Second, we approximate the relevant velocity field in Eq. (1) by that of the unperturbed flow, averaged over the particle volume. Clearly, this approximation

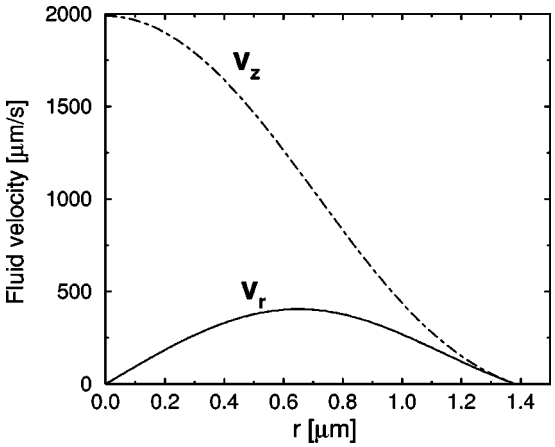

FIG. 6. Same velocity field as in Fig. 5 but depicted as a function of r at a fixed z value of $L/6$.

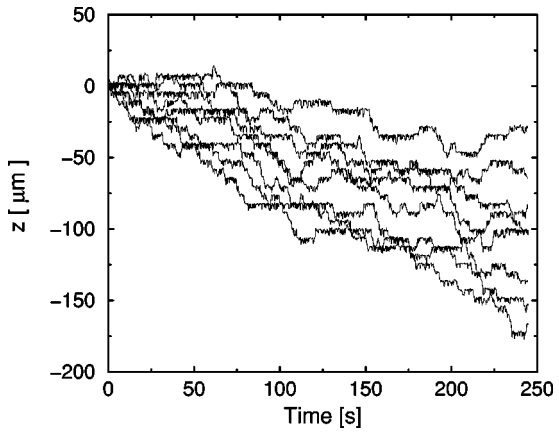

FIG. 7. Numerical simulation of the stochastic dynamics (1) with pore shape (2), $T=293$ K (room temperature), viscosity $\nu=0.5\nu_{water}$, and particle diameter $2R=0.7$ μm. The velocity field in Eq. (1) has been obtained numerically as described in Sec. III C (unperturbed velocity field, averaged over spherical particle volume) with a sinusoidal pumping of the liquid at a frequency $\omega/2\pi$ of 40 Hz. The pumping amplitude A (see main text for the exact definition) is chosen equal to the period $L=6$ μm of the ratchet-shaped pore. Depicted is the z component (along the pore axis) of the trajectory $\vec{x}(t)$ with initial condition $\vec{x}(0)\approx\vec{0}$ for eight realizations of the stochastic dynamics (1).

for the velocity field in Eq. (1) is in general not identical but of comparable quality to the approximation by the velocity field of the unperturbed flow, evaluated at the center of the spherical particle. Comparing the results when using either of these two approximations in Eq. (1) thus seems also a reasonable indicator for the deviations from the exact solution. Our simulations, as described in more detail in the next section, lead to practically indistinguishable results for both above-mentioned approximations for the velocity field in Eq. (1). We finally remark that in the limit of vanishing particle radius the diffusion coefficient in Eq. (1) diverges. The fact that our simulations still seem to approach a vanishing average particle current in this limit, in agreement with our prediction from Sec. III B, is another very strong indication of the self-consistency of our approach.

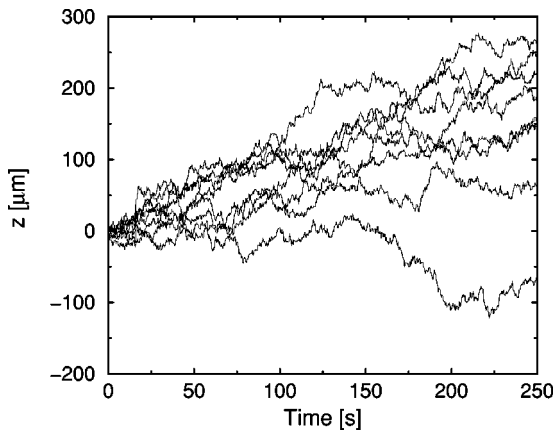

FIG. 8. Same as Fig. 7 but for a doubled pumping amplitude of $A=2L$.

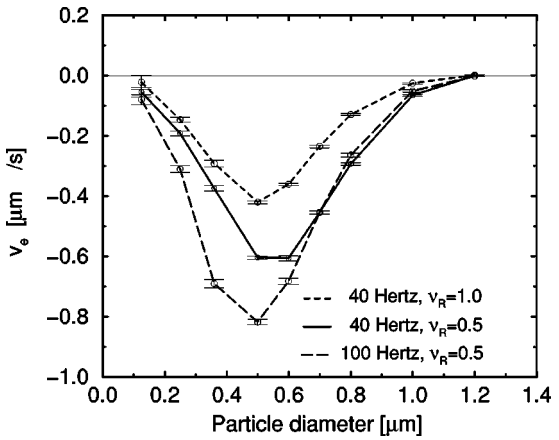

FIG. 9. Average particle current v_e from Eq. (21) versus particle diameter for various driving frequencies $\omega/2\pi$ and viscosities [cf. Eq. (20)]. Further details are as in Fig. 7.

IV. NUMERICAL SIMULATIONS

An analytical treatment of a driven three-dimensional stochastic dynamics far from equilibrium like in Eq. (1) is impossible. In this section we present and discuss results of a few representative numerical simulations with parameters that provide a reasonable description of the real experiment. While we will confine ourselves to numerical simulations of the stochastic dynamics (1), it should be mentioned that we have also cross-checked the results by numerical solutions of the associated Fokker-Planck-equation [16]. Unlike in the preceding subsection, Sec. III C, we will exclusively use dimensionful units throughout the rest of the paper.

A. Average directed particle transport

Figures 7–10 illustrate the particle motion inside a pore shaped like in Fig. 4. As pumping frequency $\omega/2\pi$ of the sinusoidal driving our standard values are $\omega/2\pi=40$ Hz and $\omega/2\pi=100$ Hz. Further, the viscosity ν of the carrier liquid is expressed in units of water viscosity, i.e., by means of the relative viscosity

$$\nu_R := \nu/\nu_{water}, \quad \nu_{water}=1.025\times 10^3\times\frac{Ns}{m^2}, \tag{20}$$

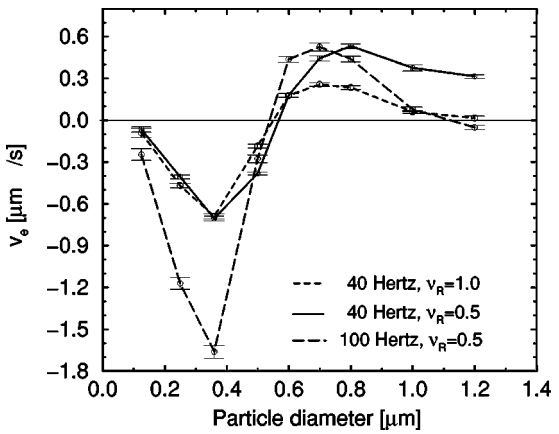

FIG. 10. Same as Fig. 9, but for a doubled pumping amplitude of $A=2L$.

with $\nu_R=0.5$ and $\nu_R=1$ as standard choices. A further parameter is the pumping amplitude A, i.e., the amplitude (maximal elongation) of the liquid around the reference position $r=z=0$.

With the numerically determined velocity field along the lines of Sec. III C as input, the Langevin equation (1) is integrated numerically in small discrete time steps, with the correspondingly discretized thermal noise supplied by a random number generator. The reflecting boundary conditions are approximately taken into account by the prescription that any step in the discretized dynamics that would lead out of the pore is replaced by a null step.

Figures 7 and 8 display results of such a numerical simulation of the stochastic dynamics (1). A systematic displacement of the particles along the pore axis in the course of time (ratchet effect) is clearly visible. Superimposed to this directed transport is a considerable diffusion-type spreading-out of the different realizations. For small driving amplitudes (Fig. 7) the particles remain within the same period of the ratchet-shaped pore for some time before they cross over to an adjacent period. For larger driving (Fig. 8) this underlying periodicity of the pores is almost completely washed out and the net particle motion is just in the opposite direction than in Fig. 7.

In the remainder of this section we discuss results that are obtained by averaging (indicated by $\langle\cdots\rangle$) over ca. 100 realizations of the stochastic dynamics (1), each evolved from $t=0$ up to the same ''running time'' $t=t_{run}$ (typically $t_{run}=250$ s). From the spread of the numerically simulated results the standard deviation can be calculated in the usual way, indicated as error bars in the plots.

Figure 9 shows the average velocity

$$v_e := \langle z(t_{run})\rangle / t_{run} \tag{21}$$

of particles in the pore for a pumping amplitude of $A=L$. As anticipated in Sec. III B, the particle velocity exhibits a distinct maximum as a function of the particle size and approaches zero for both very large and very small diameters. All particles move to the left with respect to the ratchet profile from Fig. 4. With increasing viscosity, the velocities decrease, especially for the larger particles, whereas increasing the pumping frequency $\omega/2\pi$ from 40 Hz to 100 Hz only seems to affect the smaller particles. Note that the average systematic drift per driving period of about 1/100–1/40 secs is rather small in comparison with the typical displacement of a few μm during such a period. This makes reliable numerical simulations rather time consuming.

The striking implication of the current inversion as a function of the pumping amplitude seen in Figs. 7 and 8 for the case of a variable particle diameter is depicted with Fig. 10. As compared to Fig. 9 with $A=L$, in Fig. 10 with $A=2L$, the transport direction is reversed for the larger particles; i.e., they now move through the *same* pore just in opposite direction than the smaller particles. Since in this direction (to the right in Fig. 4) the pore looks like a series of funnels, we suggest that the transport mechanism in this case may be comparable to that of an ''entropic ratchet'' [17]: The bigger particles experience many collisions with the pore walls, whose asymmetric shape apparently makes it easier for them to proceed into the funnel direction. An intuitive explanation of the transport direction for the small particles does not seem possible.

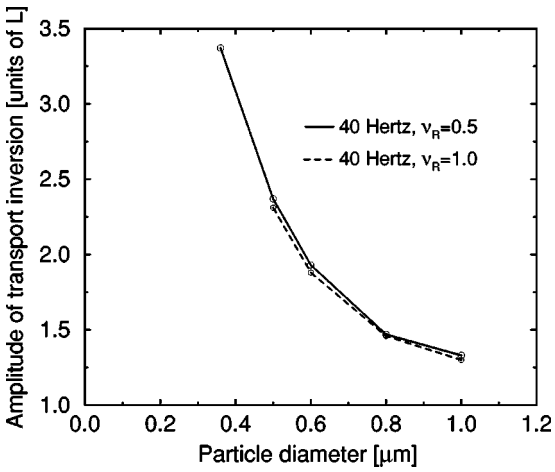

FIG. 11. The pumping amplitude A at which the particle current changes sign as a function of the particle diameter for different relative viscosities $\nu_R=\nu/\nu_{water}$. Further details are as in Fig. 7.

The occurrence of current reversals in ratchet models when certain parameters are varied has been observed and discussed before under various circumstances [3]. In our case, the current reversal is characterized by the following features: (i) It is accompanied by a rather strong variation of the current as a function of the particle diameter, (ii) the location of the reversal is very weakly dependent on the driving frequency (Fig. 10) and the relative viscosity (Fig. 11), and (iii) the maximal currents in both directions are of comparable size.

For a few shapes of the pore other than in Eq. (2) we have obtained very similar qualitative features. Furthermore, the specific particle size at which the inversion of the transport direction occurs is a function of the pumping amplitude A, as Fig. 11 shows. In principle, one still might have doubts whether the current inversion in Fig. 10 is not an artifact of our approximations for the velocity field $\vec{v}(\vec{x},t)$ form Sec. III C. Since these approximations become better and better with decreasing particle size, while in Fig. 11 the inversion point can be made to occur even for very small sizes, there remains little doubt that the current inversion is *not* an artifact of our approximations.

Altogether, the effective transport velocities exhibit extremely nonlinear behavior as a function of the particle size, which qualifies this ratchet type as an attractive candidate for a separation device.

B. Effective particle diffusion

As Figs. 7 and 8 already suggest, and as we will see in detail in the next section, besides the time- and space-averaged transport velocity v_e from Eq. (21), a further crucial quantity for the particle separation mechanism is the effective diffusion constant, i.e.,

$$D_e := [\langle z^2(t_{run})\rangle - \langle z(t_{run})\rangle^2]/2t_{run}\,. \tag{22}$$

Numerical calculations show that this definition makes sense; i.e., D_e seems to approach a well-defined, finite limit for $t_{run}\gg 2\pi/\omega$.

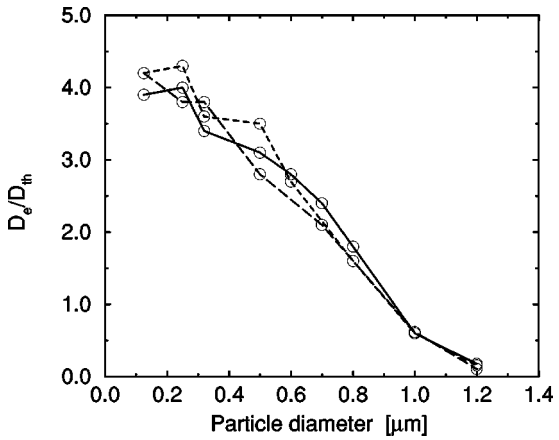

FIG. 12. The effective diffusion coefficient D_e from Eq. (22) in units of the thermal diffusion coefficient D_{th} versus particle diameter for the same parameter values as in Fig. 9.

However, the ratio D_e/D_{th} is not independent of the particle size; cf. Fig. 12: For smaller particles the effective diffusion is increased since they frequently change between liquid ''layers'' of different speeds. Larger particles develop a tendency to get trapped inside the pore cavities, yielding a reduced effective diffusion. For similar reasons, D_e/D_{th} also increases strongly as a function of the pumping amplitude A, as Fig. 13 shows.

V. MODELING FINITE PORES WITH BASINS

In this section we abandon the idealization of infinitely long pores and return to the real experimental setup with a finite pore length and adjacent liquid-plus-particle basins as indicated in Fig. 3.

A. Coarse-grained description

Assuming an initial homogeneous distribution of the particles in the liquid, how long does it take to achieve a considerable gradient in the particle density under the action of the pumping mechanism in the pore domain as described in Sec. III? The time scale of this separation process is clearly much longer than any other relevant time scale of the stochastic dynamics. On the one hand, this ''separation of time scales'' makes a direct simulation of the process practically unfeasible; on the other hand, it may be exploited as a major ingredient for deriving a much simpler approximate effective description on a coarse-grained level. The second ingredient for doing so is based on the observation that the variation of the particle density within one pore period is not of interest for our question. Neither is the density variation in the x and y directions: Inside the pores, it cannot be observed, and outside we may assume a homogeneous distribution, since there are about 1.5×10^6 pores per square centimeter of the silicon wafer.

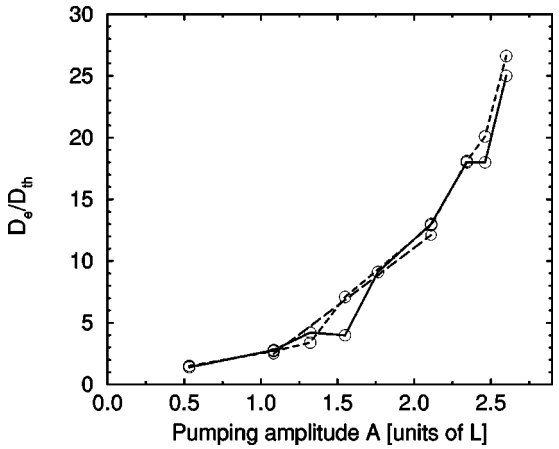

FIG. 13. The effective diffusion coefficient D_e from Eq. (22) in units of the thermal diffusion coefficient D_{th} versus pumping amplitude for a fixed particle diameter of 0.6 μm. Other parameter values are as in Fig. 9. (For the dashed lines only two data points have been computed.)

Our starting point is the time-dependent particle density $P(x,y,z,t)$. Note that this density is defined on the entire three-dimensional space, being zero outside the region which is accessible to the liquid-plus-particle suspension. Next we define a coarse-grained one-dimensional probability density $\overline{P}(n,t)$ according to

$$\overline{P}(n,t) := \frac{\omega}{2\pi L}\int_{t-\pi/\omega}^{t+\pi/\omega} dt' \int_{nL-L/2}^{nL+L/2} dz \int dx dy P(x,y,z,t'). \tag{23}$$

Thus, $\overline{P}(n,t)$ represents the one-dimensional probability density along the z axis of finding a particle in the nth ''unit cell'' of length L (summed over all the parallel pores). Inside the pores, i.e., for $-z_P \leqslant z \leqslant z_P$ in Fig. 3, $n=-n_P, \ldots, n_P$ numbers the pore periods. The total pore length is thus given by $(2n_P+1)L$. In total, n runs from $-n_B$ to n_B to cover the whole relevant z range $[-z_B, z_B]$ in Fig. 3. Note that for reasons of particle conservation, the average over time in Eq. (23) has typically only a very small effect but is included here for the sake of convenience.

In order to predict the further evolution in time of the coarse-grained density (23), knowledge of its present state $\overline{P}(n,t)$ is obviously not sufficient; one needs also a detailed distribution of particles inside each ''unit cell'' or, alternatively, knowledge of the coarse-grained density over the entire past (non-Markovian dynamics). The above-mentioned separation of time scales, however, suggests that a very accurate effective Markovian dynamics [further evolution only in terms of the present-coarse grained state $\overline{P}(n,t)$] should be possible. The situation is much like in the context of random walk theory [18], deterministic diffusion [19], Taylor dispersion [13], or nucleation [20]. For physical reasons, only transitions between neighboring cells can play a role for infinitesimal time increments; i.e., the coarse-grained dynamics has the general form of a Markovian chain model

$$\frac{\partial \overline{P}(n,t)}{\partial t} = k^+(n-1)\overline{P}(n-1,t) + k^-(n+1)\overline{P}(n+1,t) - \overline{P}(n,t)[k^+(n)+k^-(n)]. \tag{24}$$

So far, all the rates $k^{\pm}(n)$ are still undetermined model parameters. However, all but two of them are immediately fixed by the requirement that the known coarse-grained behavior inside the basins and inside the pores be correctly reproduced. Namely, we require that the average drift velocity in the pore region, i.e., $|n| \leqslant n_P$, be v_e and the effective diffusion coefficient be D_e. In the basin regions, i.e., $|n| > n_P$, we have pure thermal diffusion D_{th} and no drift in a preferential direction. [The quantitative values of v_e and D_e follow from the simulations in Sec. IV, while D_{th} is given by kT/η; see below Eq. (1).] In order to correctly reproduce these transport properties in the coarse-grained model (24), the rates are bound to take on the following values:

$$k^{\pm}(n) = \frac{D(n)}{L^2} \pm \frac{v(n)}{2L}, \tag{25}$$

$$v(n) := v_e \Theta(n_P - |n|), \tag{26}$$

$$D(n) := D_{th} + (D_e - D_{th})\Theta(n_P - |n|), \tag{27}$$

where the step function $\Theta(x)$ is 1 for $x \geqslant 0$ and 0 otherwise. This formula (25) applies to all rates with the exception of those two rates $k^{-}(n_P+1)$ and $k^{+}(-n_P-1)$ which describe the transitions from the left and right basins into the pores, respectively. Strictly speaking, the dynamics of the liquid and thus of the particles at the matching points of the pore and the basin regions is very complicated and thus the derivation of these two rates is difficult, with the exception of the fact that they are equal. Since also $k^{-}(n_P+2)$ is equal to $k^{+}(-n_P-2)$, we thus may write

$$\frac{k^{-}(n_P+1)}{k^{-}(n_P+2)} = \frac{k^{+}(-n_P-1)}{k^{+}(-n_P-2)} =: \kappa. \tag{28}$$

A reasonable approximation for this single remaining model parameter κ can be obtained as follows: neglecting the particle dynamics in the x and y directions, a particle attempting to enter the pore region will hit a pore and thus be successful with a probability that is given as the ratio of areas of all the pore cross sections and of the cross section of the basin. Thus $k^{-}(n_P+1)$ is simply reduced by this factor in comparison with the ''normal case'' $k^{-}(n_P+2)$, and similarly for $k^{+}(-n_P-1)$. In other words, we can approximately identify κ with the ratio of areas of all the pore cross sections and of the cross section of the basin. A typical value of this ratio of areas for the real experiment is

$$\kappa = 1/9. \tag{29}$$

This one-dimensional Markovian chain model (24)–(29) has also been checked by comparison to an improved three-dimensional Markovian model, which naturally is able to describe the change of accessible volume at the basin-pore transitions without a modification of the hopping rates like in Eqs. (28) and (29). The numerical results from the one-dimensional approach have been found to agree excellently with those of the three-dimensional model.

Note that the terms on the right hand side of Eq. (24) with Eqs. (25)–(28) can be rearranged into the form of a discretized Fokker-Planck equation in Ito interpretation. After taking the limit $L \to 0$ with $(2n_P+1)L = 2z_P$ and $(2n_B+1)L = 2z_B$ kept fixed, and $z := nL$, a continuous Fokker-Planck equation of the following form can be derived [16]:

$$\frac{\partial \overline{P}(z,t)}{\partial t} = \frac{\partial}{\partial z}\left\{ -v(z) + g(z)\frac{\partial}{\partial z}\frac{D(z)}{g(z)} \right\} \overline{P}(z,t), \tag{30}$$

where we introduced

$$g(z) := 1 - (1-\kappa)\Theta(z_P - |z|) \tag{31}$$

and where $v(z), D(z)$ are defined analogously to Eqs. (26) and (27). Note that (up to a normalization factor) $g(z)$ is nothing else than the area in the x-y plane that is accessible to the liquid-plus-particle suspension as a function of z. In other words, the ratio

$$\rho(z,t) := \overline{P}(z,t)/g(z) \tag{32}$$

characterizes the averaged particle concentration, i.e., the number of particles per volume of the surrounding liquid (up to an overall normalization factor and within the approximations of our coarse grained description). By closer inspection of Eq. (30) one can infer that $D(z)\,\rho(z,t)$ is continuous at the transition from the basins into the pore, whereas all other quantities like $D(z)$, $g(z)$, $\overline{P}(z,t)$, and $\rho(z,t)$ are discontinuous.

B. Particle separation

The one-dimensional model (24) can be readily solved in the steady state, i.e., in the long time limit $t \to \infty$ (superscript ''∞''):

$$\overline{P}^{\infty}(n) = \mathcal{N} \frac{\prod_{-n_B}^{n-1} k^{+}(m)}{\prod_{-n_B+1}^{n} k^{-}(m)}, \tag{33}$$

where $\mathcal{N}$ is a normalization constant. Taking into account Eqs. (25)–(28) we find that $\overline{P}^{\infty}(n)$ is constant and equal to $\overline{P}^{\infty}(n_B)$ within the entire right basin, i.e., for $n > n_P$, and similarly for the left basin, and that the ratio of these time-asymptotic particle concentrations is

$$\frac{\overline{P}^{\infty}(n_B)}{\overline{P}^{\infty}(-n_B)} = \left(\frac{1 + \dfrac{v_e L}{2D_e}}{1 - \dfrac{v_e L}{2D_e}} \right)^{2n_p+1}, \tag{34}$$

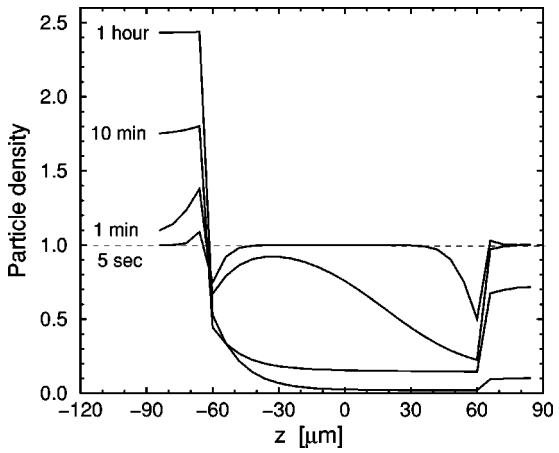

FIG. 14. Time evolution of the averaged particle density $\rho(z,t)$ from Eq. (32) by numerically solving Eqs. (24)–(29) with particle diameter 0.36 μm, $L=6$ μm, $z_P=63$ μm, $z_B=87$ μm (cf. Fig. 3). For $t=0$, the initial distribution is chosen homogeneous [$\rho(z,t=0)=1$]. The input parameters for the Langevin equation (1) are $\omega/2\pi=100$ Hz, $\nu_R=0.5$, and $A=L$, resulting in an effective transport velocity of $v_e=-0.69$ μm/s and an effective diffusion of $D_e/D_{th}=3.8$ (compare Figs. 9 and 12).

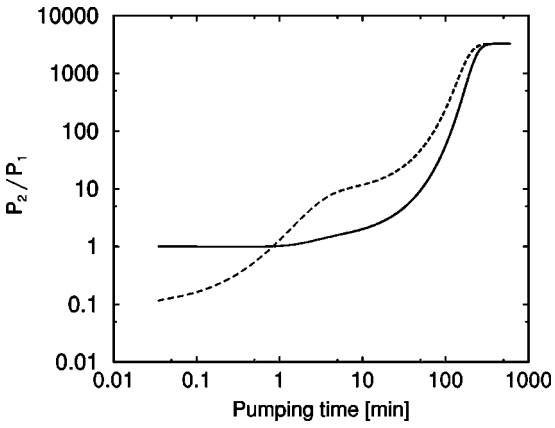

FIG. 15. Ratio $\overline{P}_2(z_B,t)/\overline{P}_1(z_B,t)=\rho_2(z_B,t)/\rho_1(z_B,t)$ of the densities for two types of particles at the border $z=z_B$ of the right basin, as a function of the pumping time, calculated from Eq. (24). Solid line: for homogeneous initial densities $\rho_{1,2}(z,t=0)$ over basins and pores. Dashed line: for homogeneous initial distribution in the pore region and vanishing densities in the basin regions. Parameters: microsphere diameters 0.36 μm and 0.7 μm, $\nu_R=0.5$, $A=2L$, $\omega/2\pi=100$ Hz, $v_e=-1.6$ and 0.54 μm/s, and $D_e/D_{th}=10.8$ and 10.5, respectively.

independent of the factor κ from Eq. (28). In the limit $L\to 0$, with $(2n_P+1)L=2z_P$ and $(2n_B+1)L=2z_B$ kept fixed, we find from Eq. (33) or, equivalently from Eq. (30) that

$$\overline{P}^{\infty}(z) = \mathcal{N}\begin{cases} 1, & -z_B \leqslant z < -z_P, \\ \kappa\dfrac{D_{th}}{D_e}\exp\left(\dfrac{(z+z_P)v_e}{D_e}\right), & -z_P \leqslant z \leqslant z_P, \\ \exp\left(\dfrac{2z_P v_e}{D_e}\right), & z_P < z \leqslant z_B. \end{cases} \tag{35}$$

The continuous expression $\overline{P}^{\infty}(z_B)/\overline{P}^{\infty}(-z_B)=\exp(2z_P v_e/D_e)$ following from Eq. (35) underestimates the ratio from Eq. (34) by an amount depending on the length scale L and the exponent $2z_P v_e/D_e$. The deviation stays below 10% for $L=6$ μm and exponents between -8 and 8. For the model parameters as used in Figs. 9 and 10, this exponent $2z_P v_e/D_e$ takes values from -23 to 0 and -8 to 7, respectively. Generally speaking, the continuous approximation (35) is useful in the parameter region where transport inversion occurs. However, for small driving amplitudes like in Fig. 9, where high transport velocities in combination with low effective diffusion may occur, the expression (33) is preferable.

C. Numerical results

For practical applications, not only are the steady state concentrations important, but also the time needed to achieve reasonably large concentration differences between the two basins. An analytical solution of Eq. (30) is still possible in the time-dependent case but involves tedious definite integrals over Gaussians. We therefore restrict ourselves to numerical solutions of the Markovian chain model (24)–(29). [Again, the agreement with solutions of Eq. (30) has been found to be very good.] Figure 14 shows how the drift ratchet works as a micropump: The averaged particle density $\rho(z,t)$ of microspheres with 0.36 μm diameter is plotted as a function of z, for different pumping times t. For $t=0$, the particles are equally distributed over the whole accessible volume in basins and pores, corresponding to $\rho(z,t=0)=1$. For $t=5$ s, two peaks appear right outside the pores. They originate from the facts that the diffusion inside the pores is stronger than outside, and that the diffusive process is dominant at small time scales. After 1 min, the pumping has caused a clear bias in the particle distribution, which becomes even more pronounced after 10 min. One hour later, a considerable concentration gradient has been built up which is already quite close to the asymptotic long-time limit.

For this calculation, the extension of the basins in the z direction was kept at a relatively small value of 24 μm. For larger basins, more time is needed to achieve similar results, because the particles have to diffusively cover a longer distance in the basins and because a larger quantity of particles has to be transported from one basin into the other until the concentration difference takes appreciable values. A certain acceleration can be achieved by stirring in the basins. However, if larger basin volumes are desirable, it is better to extend the geometry in x and y direction, thereby also increasing the number of macropores.

Figure 15 shows the separating power of our model device: Here, we started with a homogeneous suspension of an equal number of two different types of particles in the carrier liquid: The microspheres of type 1 have a diameter of 0.36 μm and those of type 2 of 0.7 μm. The input parameters are the same as before, except for the pumping amplitude of $A=2L$. The corresponding effective velocities are $v_e^{(1)}$

$=-1.6$ μm/s and $v_e^{(2)}=0.54$ μm/s, respectively (compare Fig. 10), and the effective diffusion constants are $D_e^{(1)}=10.8\,D_{th}$ and $D_e^{(2)}=10.5\,D_{th}$, respectively.

Since the smaller particles travel to the left basin and the bigger ones to the right basin, the ratio of the particle densities at the end of the right basin, $\overline{P}_2(z_B,t)/\overline{P}_1(z_B,t)$, increases with time. Note that the ratio of densities, $\rho_2(z_B,t)/\rho_1(z_B,t)$, from Eq. (32) coincides with $\overline{P}_2(z_B,t)/\overline{P}_1(z_B,t)$. The solid line shows the case of an homogeneous initial distribution of all particles throughout basins and pores $[\rho_{1,2}(z,t=0)\equiv 1]$. The dashed line corresponds to homogeneous initial distribution only within the pores, and no particles in the basins. Due to the larger diffusion of the smaller particles, the ratio $\overline{P}_2(z_B,t)/\overline{P}_1(z_B,t)$ is smaller than one in the beginning, but then the separation is somewhat faster than in the first scenario.

The steady-state ratio (long time limit) $\overline{P}_2^{\infty}(z_B)/\overline{P}_1^{\infty}(z_B)$ for an equal number of type 1 and type 2 particles can be calculated from Eq. (35). With the abbreviation $E_{1,2}:=\exp(2z_P v_e^{(1,2)}/D_e^{(1,2)})$, the ratio is given by

$$\frac{\overline{P}_2^{\infty}(z_B)}{\overline{P}_1^{\infty}(z_B)}=\frac{E_2}{E_1}, \tag{36}$$

$$\frac{(z_B-z_P)(1+E_1)+\kappa\dfrac{D_{th}^{(1)}}{v_e^{(1)}}(E_1-1)}{(z_B-z_P)(1+E_2)+\kappa\dfrac{D_{th}^{(2)}}{v_e^{(2)}}(E_2-1)}.$$

For the parameters of Fig. 15, this theoretical ratio reaches the value $\overline{P}_2^{\infty}(z_B)/\overline{P}_1^{\infty}(z_B)=2958$, which somewhat underestimates the value of 3272 found as the large time end in Fig. 15.

Note that these results were achieved without fine-tuning any parameters or optimizing the shape of the pores. For instance, for higher pumping frequencies, the transport velocities can be considerably increased, with the effective diffusion almost staying constant. This should allow an even better separation of different types of particles.

Obviously, the ability of our drift ratchet to transport particles in different directions is very useful for separation purposes. As already mentioned at the end of Sec. IV A, the particle size at which the current inversion occurs will change when the geometry of the pores, e.g., their diameter, is changed. Therefore, each macroporous silicon wafer with a certain geometry of the pores can be used as a highly accurate filter for a certain spectrum of particle sizes.

VI. SUMMARY AND OUTLOOK

In this paper we have theoretically analyzed a silicon wafer, pierced by a huge number of practically identical parallel pores with a ratchet-shaped, i.e., periodic but asymmetric, variation of the diameter along the pore axis (Figs. 1–3). The pores are filled with a liquid (e.g., water) and connected at both ends to basins and some pumping device that produces a time-periodic current of liquid back and forth through the pores. Suspended in the liquid are particles of micrometer size and the objective is to separate them according to their size into the two basins.

We have put forward a stochastic model for an idealized infinitely long and exactly periodic pore under the assumption of negligible particle inertia, gravitation effects, interactions with other particles, and interactions with the pore walls other than via the perfect reflecting boundary conditions. In the calculation of the liquid velocity field that carries the particles we have used the Navier-Stokes equation for an incompressible viscous liquid with negligible inertia terms (so-called creeping-flow approximation), justified by the small Reynolds and big Strouhal numbers arising under realistic experimental conditions. The impact of the finite particle size on the liquid velocity field has been neglected, but the effective velocity experienced by the extended particle in the inhomogeneous velocity field has been taken into account approximately.

The ratchet-shaped pore profile in conjunction with the far-from-equilibrium situation created by the periodically alternating velocity field of the liquid gives rise to a ratchet effect, i.e., a net particle transport along the pore axis, although both the external force of the streaming liquid and the thermal noise average out to zero. The basic physical mechanism for the emergence of such a nonvanishing net particle current is the thermal diffusion between ''liquid layers'' of different speed—similar to Taylor dispersion [13]—and the collisions with the pore walls. Through the asymmetry of the pore profile an asymmetry between pumping forth and back arises for both the thermal interlayer diffusion and the collisions with the pore walls, resulting in a nonvanishing particle displacement on average after one driving period. The fact that the excursions of the particles during one driving period are typically much larger than the net displacement after one period motivates the name ''drift ratchet.'' It may also be worth noting that in biological systems where substances are transported in determined directions along so-called microtubuli, the achieved velocities of about 1 μm/s are of the same order of magnitude as those predicted for our setup.

The dependence of the magnitude and even the direction of the net particle current upon the particle size is difficult to predict intuitively. The numerically observed sensitive dependence of the current direction on the particle size (Fig. 10) appears to be a quite robust feature of this class of diffusion ratchets. In particular, an exact spherical shape of the particles does not seem necessary.

For a real silicon wafer with pores of finite length, connected at both ends with liquid-plus-particle reservoirs, we have introduced a coarse-grained description, based on an approximate but apparently fairly faithful Markovian assumption, with the result of an effective one-dimensional Markovian chain model, quite similar to the coarse-grained models employed in various other contexts [13,18–20]. The model parameters in this effective description can be determined either through the ''first principles'' Langevin approach from Secs. III and IV or by fitting with the real experiment. For a realistic choice of parameters our numerical and analytical calculations predict a surprisingly high sepa-

rating power of the device with a remarkable resolution with respect to particle size (Figs. 14 and 15).

As a generalization of the original setup from Fig. 3 one may also consider an alternating sequence of several basins and silicon wafers with different pore characteristics. In this way, more than two types of particles could be separated within a single run by accumulating them in a controlled way inside the different basins.

ACKNOWLEDGMENTS

C.K. and P.H. gratefully acknowledge financial support by the BMBF under Contract No. 13N7121. P.R. and P.H. wish to thank the German National Science Foundation under Grant No. DFG-Sachbeihilfe HA1517/13-2 and the Graduiertenkolleg GRK283 ''Nonlinear Problems in Analysis, Geometry, and Physics.''

[1] M.v. Smoluchowski, Phys. Z. **13**, 1069 (1912); R.P. Feynman, R.B. Leighton, and M. Sands, *The Feynman Lectures on Physics* (Addison-Wesley, Reading, MA, 1963), Vol. 1, Chap. 46; J.M.R. Parrondo and P. Espanol, Am. J. Phys. **64**, 1125 (1996).

[2] A. Ajdari and J. Prost, C. R. Acad. Sci. (Paris) **315**, 1635 (1992); M.O. Magnasco, Phys. Rev. Lett. **71**, 1477 (1993); R.D. Astumian and M. Bier, *ibid.* **72**, 1766 (1994).

[3] For reviews see P. Hänggi and R. Bartussek, in *Lecture Notes in Physics*, edited by J. Parisi *et al.* (Springer, Berlin, 1996), Vol. 476; R.D. Astumian, Science **276**, 917 (1997); F. Jülicher, A. Ajdari, and J. Prost, Rev. Mod. Phys. **69**, 1269 (1997).

[4] R.D. Vale and F. Oosawa, Adv. Biophys. **26**, 97 (1990).

[5] B.I. Sturman and V.M. Fridkin, *The Photovoltaic and Photorefractive Effects in Noncentrosymmetric Materials* (Gordon and Breach, Philadelphia, 1992).

[6] S. Leibler, Nature (London) **370**, 412 (1994).

[7] J. Rousselet, L. Salome, A. Ajdari, and J. Prost, Nature (London) **370**, 446 (1994); L.P. Faucheux, L.S. Bourdieu, P.D. Kaplan, and A.J. Libchaber, Phys. Rev. Lett. **74**, 1504 (1995); L. Gorre, E. Ioannidis, and P. Silberzan, Europhys. Lett. **33**, 267 (1996); L. Gorre-Talini and P. Silberzan, J. Phys. I **7**, 1475 (1997); L. Gorre-Talini, S. Jeanjean, and P. Silberzan, Phys. Rev. E **56**, 2025 (1997); H. Linke *et al.*, Europhys. Lett. **44**, 343 (1998); **45**, 406(E) (1999); A. Lorke *et al.*, Physica B **249**, 312 (1998); L. Gorre-Talini, J.P. Spatz, and P. Silberzan, Chaos **8**, 650 (1998); C. Mennerat-Robilliard *et al.*, Phys. Rev. Lett. **82**, 851 (1999); O. Sandre, L. Gorre-Talini, A. Ajdari, J. Prost, and P. Silberzan, Phys. Rev. E **60**, 2964 (1999); S. Weiss, D. Koelle, J. Müller, K. Barthel, and R. Gross, Phys. Rev. Lett. (to be published); J.S. Bader, R.W. Hammond, S.A. Henck, and M.W. Deem (unpublished); R.W. Hammond, J.S. Bader, S.A. Henck, M.W. Deem, G.A. McDermott, J.M. Bustillo, and J.M. Rothberg (unpublished).

[8] *Electrophoresis of Large DNA Molecules—Theory and Applications*, edited by E. Lai and B.W. Birren (Cold Spring Harbor Laboratory Press, New York, 1990).

[9] J.C. Giddings, Sep. Sci. **1**, 123 (1996); H.C. Berg and E.M. Purcell, Proc. Natl. Acad. Sci. USA **58**, 862 (1967); **58**, 1286 (1967); , **58**, 1821 (1967); C. Van den Broeck and D. Maes, Sep. Sci. Technol. **22**, 1269 (1987).

[10] V. Lehmann and H. Föll, J. Electrochem. Soc. **137**, 653 (1990); V. Lehmann, *ibid.* **140**, 2836 (1993); V. Lehmann and U. Grüning, Thin Solid Films **297**, 13 (1997); S. Ottow, V. Lehmann, and H. Föll, J. Electrochem. Soc. **143**, 385 (1996).

[11] R. Bartussek, P. Hänggi, and J.G. Kissner, Europhys. Lett. **28**, 459 (1994); A. Ajdari, D. Mukamel, L. Peliti, and J. Prost, J. Phys. I **4**, 1551 (1994); P. Reimann, R. Bartussek, R. Häussler, and P. Hänggi, Phys. Lett. A **215**, 26 (1996); I. Zapata, R. Bartussek, F. Sols, and P. Hänggi, Phys. Rev. Lett. **77**, 2292 (1996); J. Plata, Phys. Rev. E **57**, 5154 (1998).

[12] K.M. Jansons and G.D. Lythe, Phys. Rev. Lett. **81**, 3136 (1998); D.E. Postnov, A.P. Nikitin, and V.S. Anishchenko, Phys. Rev. E **58**, 1662 (1998); M. Borromeo and F. Marchesoni, Phys. Lett. A **249**, 199 (1998); C. Van den Broeck, Europhys. Lett. **46**, 1 (1999).

[13] G.I. Taylor, Proc. R. Soc. London, Ser. A **219**, 186 (1953); I. Claes and C. Van den Broeck, J. Stat. Phys. **70**, 1215 (1993), and further references therein.

[14] L.G. Leal, *Laminar Flow and Convective Transport* (Butterworth-Heinmann, Boston, 1992); Z.U.A. Warsi, *Fluid Dynamics* (CRC Press, Boca Raton, FL, 1992).

[15] For instance, in the real experimental setup with finite pore length from Fig. 3, the pressure at the pore ends is expected to be more or less constant over the entire pore cross section.

[16] H. Risken, *The Fokker-Planck Equation* (Springer, Berlin, 1984).

[17] G.W. Slater, H.L. Guo, and G.I. Nixon, Phys. Rev. Lett. **78**, 1170 (1997).

[18] G.H. Weiss, *Aspects and Applications of the Random Walk* (North-Holland, Amsterdam, 1994).

[19] H. Fujisaka and S. Grossmann, Z. Phys. B: Condens. Matter **48**, 261 (1982); T. Geisel and J. Nierwetberg, Phys. Rev. Lett. **48**, 7 (1982); M. Schell, S. Fraser, and R. Kapral, Phys. Rev. A **26**, 504 (1982).

[20] V.A. Shneidman and P. Hänggi, Phys. Rev. E **49**, 894 (1994).